1	Chemical composition, optical properties, and oxidative potential of water-
2	and methanol-soluble organic compounds emitted from the combustion of
3	biomass materials and coal
4	
5	Tao Cao ^{1,2,3} , Meiju Li ^{1,2,3} , Chunlin Zou ^{1,2,3} , Xingjun Fan ⁴ , Jianzhong Song ^{1,2,5,*} , Wanglu, Jia ^{1,2} ,
6	Chiling Yu ^{1,2} , Zhiqiang Yu ^{1,2} , Ping'an Peng ^{1,2,3,5}
7	
8	¹ State Key Laboratory of Organic Geochemistry and Guangdong Provincial Key Laboratory
9	of Environmental Protection and Resources Utilization, Guangzhou Institute of Geochemistry,
10	Chinese Academy of Sciences, Guangzhou 510640, China
11	² CAS Center for Excellence in Deep Earth Science, Guangzhou, 510640, China
12	³ University of Chinese Academy of Sciences, Beijing 100049, China
13	⁴ College of Resource and Environment, Anhui Science and Technology University, Anhui
14	233100, China
15	⁵ Guangdong-Hong Kong-Macao Joint Laboratory for Environmental Pollution and Control
16	
17	*Correspondence to: Jianzhong Song (songjzh@gig.ac.cn)

19 Abstract

Biomass burning (BB) and coal combustion (CC) are important sources of brown carbon 20 (BrC) in ambient aerosols. In this study, six biomass materials and five types of coal were 21 combusted to generate fine smoke particles. The BrC fractions, including water-soluble 22 organic carbon (WSOC), humic-like substance-carbon (HULIS-C), and methanol-soluble 23 organic carbon (MSOC), were subsequently fractionated, and their optical properties and 24 chemical structures were then comprehensively investigated using UV-visible spectroscopy, 25 nuclear (¹H-NMR), magnetic resonance spectroscopy and proton fluorescence 26 extraction-emission matrix spectroscopy (EEM) combined with parallel factor analysis 27 (PARAFAC). In addition, the oxidative potential (OP) of BB and CC BrC was measured with 28 the dithiothreitol (DTT) method. The results showed that WSOC, HULIS-C, and MSOC 29 30 accounted for 2.3%–22%, 0.5%–10%, and 6.4%–73% of the total mass of combustion-derived smoke PM_{2.5}, respectively, with MSOC extracting the highest 31 concentrations of organic compounds. The MSOC fractions had the highest light absorption 32 capacity (mass absorption efficiency at 365 nm ((MAE₃₆₅): 1.0–2.7 m²/gC) for both BB and 33 CC smoke, indicating that MSOC contained more of the strong light-absorbing components. 34 Therefore, MSOC may represent the total BrC better than the water-soluble fractions. Some 35 significant differences were observed between the BrC fractions emitted from BB and CC 36 with more water-soluble BrC fractions with higher MAE₃₆₅ and lower absorption Ångström 37 exponent values detected in smoke emitted from BB than from CC. EEM-PARAFAC 38 identified four fluorophores: two protein-like, one humic-like, and one polyphenol-like. The 39 protein-like substances were the dominant components of WSOC (47%-80%), HULIS-C 40

41	(44%–87%), and MSOC (42%–70%). The ¹ H-NMR results suggested that BB BrC contained
42	more oxygenated aliphatic functional groups (H-C-O) whereas CC BrC contained more
43	unsaturated fractions (H-C-C = and Ar-H). The DTT assays indicated that BB BrC generally
44	had a stronger oxidative potential (DTT _m , 2.6–85 pmol/min/ μ g) than CC BrC (DTT _m , 0.4–11
45	pmol/min/ μ g), with MSOC having a stronger OP than WSOC and HULIS-C. In addition,
46	HULIS-C contributed more than half of the DTT activity of WSOC ($63.1\% \pm 15.5\%$),
47	highlighted that HULIS was a major contributor of ROS production in WSOC. Furthermore,
48	the Principal component analysis and Pearson correlation coefficients indicated that highly
49	oxygenated humic-like fluorophore C4 may be the important DTT active substances in BrC.

50

51

53 **1. Introduction**

Brown carbon (BrC) is an organic compound with strong light absorption at ultraviolet 54 and short visible wavelengths and is abundant in ambient aerosols (Chen and Bond, 2010; 55 Laskin et al., 2015; Alexander et al., 2008), rain, clouds, and fog water (Santos et al., 2009; 56 Santos et al., 2012; Izhar et al., 2020). Due to its strong light absorption ability, BrC can 57 affect the radiative balance of aerosol and photochemical reactions in the atmospheric 58 environment (Andreae and Gelencser, 2006; Kumar et al., 2018a; Nozière et al., 2011). 59 Moreover, BrC has the ability to catalyze the generation of reactive oxygen species (ROS), 60 61 which potentially have an adverse impact on human health (Bates et al., 2019; Ma et al., 2018; Fan et al., 2018; Chen et al., 2019). 62

Brown carbon originates from various sources, including primary emission sources, such 63 as biomass burning (BB), coal combustion (CC), and vehicular emissions (Fan et al., 2018; Li 64 et al., 2018; Chen et al., 2019; Sun et al., 2017); and secondary processes, such as reactions 65 between carbonyls and ammonia or amines and the photochemical transformation of volatile 66 67 organic compounds (Evangeliou et al., 2019; Lin et al., 2015). Among these sources, BB and CC are considered to make significant contributions to atmospheric BrC materials as 68 indicated in both laboratory and field studies (Li et al., 2018; Park and Yu, 2016; van der Werf 69 et al., 2010; Yan et al., 2015). For example, BrC fractions, such as water-soluble organic 70 carbon (WSOC), humic-like substance-carbon (HULIS-C), and methanol-soluble organic 71 carbon (MSOC), have been found to be abundant in fresh emissions from the burning of crop 72 straw, wood branches, and coals (Park and Yu, 2016; Fan et al., 2018; Li et al., 2018; Huo et 73 al., 2018). These studies have also demonstrated that the chemical properties of primary BrC 74

are variable due to the inherent heterogeneity and complexity of fuel materials and 75 combustion conditions (Huo et al., 2018; Fan et al., 2018; Li et al., 2018; Atwi et al., 2021). 76 For example, the light absorption properties of primary HULIS-C produced by the 77 combustion of three types of crop straw under different moisture contents and stacking modes 78 are different. The absorption Ångström exponent (AAE) increased and the mass absorption 79 efficiency at 365 nm (MAE₃₆₅) decreased under high moisture or stacking conditions (Huo et 80 al., 2018). The water-soluble BrC emitted from low maturity CC generally had relatively low 81 MAE₃₆₅ values (Li et al., 2018). However, most of these studies only focused on the relative 82 83 abundances, chemical composition, and optical properties of water-soluble BrC (e.g., HULIS) emitted from the combustion of various fuels and different combustion conditions (e.g., 84 smoldering and flaming) (Huo et al., 2018; Park et al., 2016; Fan et al., 2016). It is noted that 85 86 water-insoluble BrC even exhibits a higher light absorption than water-soluble BrC in ambient aerosols (Chen et al., 2016, 2017; Bai et al., 2020; Huang et al., 2020; Li et al., 2019). 87 However, knowledge on the chemical and optical properties of water-insoluble BrC from 88 combustion sources is still lacking. Moreover, the association of chemical compositions 89 responsible for light absorption of BrC from combustion sources is still constrained. 90 Therefore, to gain more detailed information on BrC from combustion sources, a 91 comprehensive characterization, including the chemical and optical characteristics of the BrC 92 fractions (including both water-soluble and water-insoluble BrC) from the combustion of 93 biomass materials and coals, is required. 94

In addition, the oxidative potential (OP) of water-soluble organic fractions (WSOC and
HULIS) and the water-insoluble organic fraction in ambient aerosols have been investigated,

and all are known to be significant redox-active organic compounds associated with ROS 97 generation, which can adversely affect human health (Moufarrej et al., 2020; Bates et al., 98 99 2019; Verma et al., 2012; Kramer et al., 2016; Wong et al., 2019). As important contributors to ambient BrC, combustion-derived BrC is expected to have a strong ROS generation 100 capacity and be harmful to human health. For example, the oxidative potential of the 101 water-soluble fraction of atmospheric fine aerosols were analyzed and revealed that biomass 102 burning dominates the ROS-generation potential in winter, contributing more than 46% to 103 DTT activities in the southeastern United State (Verma et al., 2014) and 41% in Milan, Italy 104 105 (Hakimzadeh et al., 2020). In addition, study on the oxidative potential of water-soluble HULIS in fine aerosols in Beijing also indicated that combustion sources contributed a high 106 proportion to the oxidative stress of water-soluble HULIS fractions (Ma et al., 2018). 107 108 However, these results were mainly obtained based on the source apportionment receptor model (positive matrix factorization (PMF) and chemical mass balances (CMB)). Recently, 109 the water extracts and HULIS from biomass burning were directly investigated and presented 110 significant oxidative potential to generate ROS (e.g., 6.6-55 pmol/min/µg for WSOC and 111 HULIS extracted from biomass burning smoke) (Fan et al., 2018; Pietrogrande et al., 2021; 112 Seo et al., 2020). In addition, high oxidative potentials (2.04-15.5 pmol/min/ug) were also 113 observed for water extracts in soots generated from the combustion of fossil fuels (Li et al., 114 2019; Zhu et al., 2019). However, this limited studies only focused on the water-soluble BrC 115 fraction from biomass burning; and knowledge on the oxidative potential of the 116 water-insoluble BB BrC and BrC fractions emitted from other combustion processes, such as 117 coal combustion, is still lacking. In addition, the DTT activities of BrC from different 118

119 combustion sources were generally different, but the key components or functional groups120 that responsible for the ROS generation capacity of combustion-derived BrC are unclear.

Biomass fuels and coals are two traditional sources of energy in residential properties in 121 some developing countries, especially China and India (Sun et al., 2017; Huo et al., 2018; 122 Singh et al., 2021). Due to incomplete combustion and poor pollution control, BB and CC 123 release various pollutants, including particulate matter (PM), elemental carbon (EC), and BrC. 124 In this study, we investigated the optical properties, chemical composition, and oxidative 125 potential of BrC fractions in smokes emitted from BB and CC. Six biomass materials (three 126 types of crop straw and three types of wood branches) and five coals with different maturities 127 were combusted, and the resulting smoke particles were collected in a laboratory combustion 128 chamber. The water soluble (WSOC and HULIS-C) and methanol soluble (MSOC) fractions 129 130 in smoke were fractionated using pure water combined with solid-phase extraction (SPE) and methanol extraction. Subsequently, their chemical and optical properties were measured using 131 a total organic carbon analyzer, UV-visible spectroscopy, fluorescence extraction-emission 132 matrix spectroscopy (EEM) combined with parallel factor analysis (PARAFAC), and proton 133 nuclear magnetic resonance spectroscopy (¹H-NMR). Moreover, the oxidative potential of the 134 BrC fractions was determined by a dithiothreitol (DTT) assay. This is a comprehensive study 135 of the chemical and optical properties of BrC fractions, including both water-soluble and 136 water-insoluble fractions from BB and CC. The OP of different BrC fractions from BB and 137 CC were directly determined, and the key components or properties associated with the OP of 138 BrC were further discussed. The information obtained will enhance our understanding of the 139 chemical composition, light absorption, fluorophores, and DTT activity of the primary BrC 140

from BB and CC and could be used to estimate the environmental and climate impacts ofdifferent types of combustion-derived BrC.

143

144 **2. Materials and methods**

145 **2.1. The BB and CC smoke samples**

In this study, six biomass materials and five types of coal were collected and used to 146 generate smoke samples. The biomass materials consisted of three types of crop straw (wheat 147 straw (WS), rice straw (RS), and corn straw (CS)) and three types of wood branches (pine 148 149 wood (PW), Chinese fir (CF), and white poplar (WP)). These materials are usually used as fuels for heating and cooking in rural areas and are also occasionally burned in the field (Fan 150 et al., 2018; Kumar et al., 2018b). The combustion of these crop straws and woody fuels is 151 152 reported to make a significant contribution to atmospheric aerosols in China (Shen et al., 2013). Five types of coal were used for the collection of CC smoke samples. They consisted 153 of four types of bituminous coal (B-1, B-2, B-3, and B-4) and one anthracite coal (AN), 154 representing the major types of coal used for residential CC in China. The details of these 155 samples are provided in the supporting information (SI). 156

Samples of the smoke emitted from BB and CC were collected in a combustion and
sampling system. The system consisted of a combustion hood, clean background air dilution
and injection ports, smoke pipe, mixing fan, mixing chamber, PM_{2.5} sampler (JCH-120F,
Juchuang Environmental Protection Group Co., Ltd., Shandong, China), and an exhaust port.
The details of the sampling procedure are described in our previous study (Fan et al., 2018; Li
et al., 2018) and the SI file.

Blank quartz filters were collected before each group of combustion experiments prior to 163 the fuels being ignited. Blank filters were used to correct the mass of smoke, the optical 164 signals and DTT consumption by BrC. To prevent contamination of the following sample, the 165 collection system was cleaned before each new combustion experiment. 166

167

168

2.2. Extraction and isolation of BrC fractions

In this study, the WSOC, HULIS-C, and MSOC fractions were obtained using the 169 solvent extraction method, as described in our previous studies (Fan et al., 2016; Li et al., 170 171 2018). Initially, the filter samples were cut into small pieces and ultrasonically extracted three times with 20 mL ultrapure water for 30 min. The extract was filtered through a 0.22 µm 172 polytetrafluoroethylene (PTFE) syringe filter (Jinteng, Tianjin, China), which collected the 173 174 WSOC fraction. The HULIS-C fraction in WSOC was further isolated using the SPE (Oasis HLB, 200 mg, Waters, Milford, MA, USA) method. The detailed procedure is provided in S3 175 of SI file. 176

177 The MSOC fraction was obtained using a method developed by Cheng et al. (2016). Briefly, a portion of the filter was immersed in methanol (Macklin, >99.9%, Shanghai, China) 178 for 2 h and then filtered through a 0.22 µm PTFE syringe filter. Static digestion without 179 ultrasonic treatment can avoid the loss of PM and facilitate the determination of the dissolved 180 organic matter (DOM) content. Finally, the residual filters were dried in a vacuum dryer. The 181 OC content of MSOC was obtained by subtracting the OC concentration of the extracted 182 filters from untreated filters. 183

184

185 **2.3. UV-visible spectroscopy**

The UV-visible absorption spectra of the BrC solutions were analyzed using a UV-vis spectrophotometer (UV-2600, Shimadzu, Kyoto, Japan). The BrC solution was placed in a 0.01 m quartz cuvette, and the UV-vis spectra were recorded from 200 to 700 nm at 1 nm intervals. Milli-Q water was used as a blank reference for the WSOC and HULIS-C solutions while pure methanol was used as the blank for the MSOC fraction. The corresponding background was used to determine the interference from the instrument and operational blank sample.

To describe the optical properties of BrC fractions, the AAE and MAE₃₆₅ were calculated in this study. The AAE is a measure of the spectral dependence of chromophores in BrC while the MAE₃₆₅ can indicate the light absorbing capacity of BrC (Fan et al., 2016; Cheng et al., 2016). The detailed calculations are described in the SI file.

197

198 2.4. Fluorescence EEM spectroscopy and the PARAFAC model

The EEM fluorescence spectra of BrC fractions were recorded by an F-4600 199 fluorescence spectrometer (Hitachi, Tokyo, Japan) using a 0.01 m width quartz cuvette with a 200 400 V xenon lamp at room temperature and a 2400 nm/min scanning speed. The scanning 201 ranges for excitation (E_X) and emission (E_M) were 200–400 nm and 290–520 nm, respectively. 202 The slit width and intervals for E_X and E_M were both set to 5 nm. According to the different 203 solvents used for sample extraction (water and methanol), all EEM spectra were divided into 204 205 two groups for analysis (66 samples for water-soluble WSOC and HULIS-C and 33 samples for MSOC). The PARAFAC modeling procedure was conducted in EFC v1.2, which is an 206

application software based on MATLAB that has the functions of conversion, correction, 207 cognition, comparison, and calculation for processing the fluorescence spectra (He and Hur, 208 2015; Murphy et al., 2011; Murphy et al., 2013). The PARAFAC analysis method that was 209 included in the software was consistent with the calculation made by the drEEM toolkit when 210 using MATLAB (Murphy et al., 2010; Murphy et al., 2013). The PARAFAC was computed 211 using two to seven component models, with nonnegativity constraints and a residual analysis; 212 and split half analysis was used to validate the number of fluorescence components. 213 According to the results of the split-half and core consistency analysis, four component 214 215 models were chosen for both the WSOC and HULIS-C fractions and the MSOC. The EEM was normalized to the area under the ultrapure water Raman peak ($E_X = 350$ nm, $E_M = 365$ -216 430 nm) collected before the measurement of samples to produce corrected fluorescence 217 218 intensities in Raman units (Lawaetz and Stedmon, 2009). The relative contribution of individual chromophores was estimated by calculating the maximum fluorescence intensities 219 (F_{max}: maximum fluorescence intensity of identified fluorescence components, relative 220 content % = $F_{max}/\Sigma F_{max}$) (Matos et al., 2015; Chen et al., 2016). 221

222

223 2.5. Proton-NMR spectroscopy

Approximately 5 mg of the BrC fractions (i.e., HULIS-C, WSOC, and MSOC) derived from BB and CC were used for ¹H NMR measurements. The water-soluble BrC fractions (WSOC and HULIS-C) were redissolved in 500 μ L deuterium oxide, and MSOC was redissolved in 500 μ L deuterated methanol and then transferred to a 5 mm NMR tube. ¹H-NMR spectra were obtained at a frequency of 400 MHz using a spectrometer (Avance III 400, Bruker Daltonik GmbH, Bremen, Germany). Data were acquired from 100 scans, with a recycling time of 2 s for a condensed water sample. The length of the proton 90° pulse was $8.87 \mu s$. A 1.0 Hz line-broadening weighting function and baseline correction were applied. The identification of the functional groups in the NMR spectra was based on their chemical shift (δH) relative to that of tetramethylsilane (0 ppm), which was applied as an internal standard (Zou et al., 2020).

235

236 **2.6. Oxidative potential**

237 The oxidative potential of BrC emitted from the BB and CC processes (i.e., WSOC, HULIS-C, and MSOC) was measured by a DTT assay. This protocol was mainly followed the 238 methods introduced by Fan et al (2018) and Gao et al (2020), and also with some minor 239 240 modifications. Briefly, 3 mL of extracted sample solution (MSOC was a mixture of 100 µL sample and 2.9 mL of 18.2 MΩ Milli-Q water, and the corresponding blank was the same 241 solution as that of the water blank) and 3 mL of 1 mM DTT were mixed in a 20 mL brown 242 vial and then placed in a 37 $\,^{\circ}$ C water bath to maintain the samples at a constant temperature. 243 At specific time intervals (0, 5, 10, 15, and 20 min), 1 mL of the well-mixed sample was 244 transferred to another 4 mL brown vial, and 1 ml trichloroacetic acid (TCA 1% w/v) was 245 added to stop the reaction. Then, 0.5 mL 5,5'-dithiobis-(2-nitrobenzoic acid) (DTNB, 1 mM) 246 was added to react with the remaining DTT to produce 2-nitro-5-thiobenzoic acid (TNB). 247 After 5 min, 1 mL of tris(hydroxymethyl)methyl aminomethane buffer (0.4 mM Tris buffer, 248 pH 8.9 in 4 mM) containing diethylene triamine pentaacetic acid (DTPA) was added, and the 249 yellow color of TNB was visible in the mixed samples. The absorbance was measured at 412 250

nm with a UV-vis spectrometer (UV2600, Shimadzu). The DTT, TCA, and DTNB were all 251 dissolved in 0.1 M phosphate buffer (pH 7.4) containing 1 mM DTPA. and the corresponding 252 253 filter blank was analyzed to correct the DTT activity of the sample fractions. The DTT consumption rate after subtracting the field blank was determined using the absorbance and 254 normalized by the particulate mass (DTT_m, pmol/min/µg) (Verma et al., 2012; Fan et al., 255 2018). In this study, 1.4-phenanthraquinone was used to conduct a positive control, of which 256 the DTT consumption rate was $0.46 \pm 0.03 \mu M$ DTT/min (n=10). The rate was similar to 257 those reported in the previous studies (Fan et al., 2018; Lin and Yu, 2019). 258

Finally, principal component analysis (PCA) was performed to investigate the key factors that may affect the DTT activities from a series of characteristic of BrC fraction. The details are described in S6 of SI file.

262

263 **3. Results and discussion**

264 **3.1.** Abundance of WSOC, HULIS-C, and MSOC in BB and CC smoke samples

Table 1 summarizes the abundance of BrC fractions, including WSOC, HULIS-C, and 265 MSOC, in BB and CC smoke PM_{2.5} samples. As shown in Table 1, the average contribution 266 of WSOC to smoke PM_{2.5} was 2.9%–12% and 2.3%–22% for BB and CC, respectively. These 267 results were comparable to the results obtained for smoke samples from the combustion of 268 cherry leaves (16%), gingko tree leaves (6.0%) (Park et al., 2013), corn straw (5.9%), pine 269 branches (6.4%) (Fan et al., 2016), and residential coals (4%–11%) (Li et al., 2018) and in the 270 ambient PM_{2.5} from rural and urban sites (4–13%) (Matos et al., 2015; Qin et al., 2018; Wu et 271 al., 2020). This suggests that both BB and CC can release substantial amounts of 272

water-soluble BrC into atmospheric aerosols. As the hydrophobic fraction of WSOC, the 273 carbon content of HULIS (HULIS-C) accounted for 1.0%-7.8% and 0.5%-10% of BB and 274 275 CC smoke PM_{2.5}, respectively. These values are comparable to the results obtained for BB smoke (5.9%–15.2%) (Fan et al., 2018; Huo et al., 2018), CC smoke (1.9%–4.8%) (Li et al., 276 277 2018), and atmospheric aerosols in Beijing (4.8%–9.4%) (Li et al., 2019), with an average value of 7.2% \pm 3.3%, therefore confirming the important contributions made by BB and CC 278 to atmospheric HULIS. As a comparison, the contribution of MSOC to smoke PM_{2.5} was 279 6.4%–47% and 9.4%–73% for BB and CC, respectively, with both values being much higher 280 281 than the contributions of the water-soluble fractions (WSOC and HULIS-C) in the same smoke samples. Similar results have been reported in previous studies (Li et al., 2018; Cheng 282 et al., 2016), which suggest that there are more organic compounds that could be extracted by 283 284 methanol than by water, and it could therefore be a better indicator of total BrC. This result also indicated that BB and CC both released large amounts of water-insoluble BrC 285 compounds, including hydrophobic polycyclic aromatic hydrocarbons (PAHs) and 286 nitrogen/sulfur-containing heteroatomic PAHs (Geng et al., 2014; Dong et al., 2021; Huang et 287 al., 2020). 288

Some differences were observed among the different types of smoke samples. As shown in Figure 1, the average contributions of the WSOC and HULIS-C fractions to the total carbon (TC) were $22\% \pm 7.3\%$ and $11\% \pm 3.8\%$, respectively, for BB smoke, which were higher than the corresponding values of $19\% \pm 9.4\%$ and $8.2\% \pm 4.0\%$ for CC smoke. The contribution of MSOC to OC was $69\% \pm 19\%$ for BB, which was significantly lower than the value of $97\% \pm 1.8\%$ for CC. These results suggested that BB generally released the more

water-soluble OC fraction whereas more water-insoluble OC fraction was contained in the smoke particles emitted from CC. These differences can be explained by the fact that biomass fuels generally contain large amounts of biopolymers, such as carbohydrates (cellulose, hemicellulose, etc.); the burning of biomass fuels produces more highly polar compounds, such as phenols, polyols, and polysaccharides; and CC emits more relatively hydrophobic and less polar components, such as coal tar and polycyclic aromatic species (Wu et al., 2014; Wu et al., 2021; Huang et al., 2020).

302

303 3.2 Light absorption

AAE and MAE₃₆₅ are important optical indicators of the light absorption properties of 304 atmospheric BrC and were investigated for BB- and CC-derived BrC in this study. As shown 305 306 in Figures 2a and c, the AAE values of the WSOC and HULIS-C fractions were 6.1-9.9 (mean 7.8 \pm 1.6) and 7.2–9.6 (mean 8.5 \pm 0.8), respectively, for BB smoke and 8.5–16 (mean 307 13 \pm 2.9) and 10–16 (mean 14 \pm 2.3), respectively, for CC smoke. These results were 308 309 comparable to those measured for combustion-emitted aerosols with reported AAE values for HULIS of 7.4-8.3 (Park and Yu, 2016) and 6.2-8.1 (Fan et al., 2016, 2018) for BB smoke and 310 5.2-14 for CC smoke (Li et al., 2019). Moreover, the AAE values of BB WSOC and HULIS 311 were also comparable to those reported for WSOC in urban aerosols in Beijing (mean 7.28 \pm 312 0.24) (Cheng et al., 2016), HULIS in Amazon BB aerosols (~7.10) (Hoffer et al., 2006), 313 urban aerosols in Beijing (5.3-5.8) (Yan et al., 2015), and aerosols in the Tibetan Plateau 314 (7.14–9.35) (Wu et al., 2020) but higher than that (1.2–5.4, mean of 3.2) of water-soluble BrC 315 in Los Angeles (Zhang et al., 2013). However, the AAE values of the water-soluble BrC 316

fraction from CC were almost higher than those in ambient aerosols, as described above. The 317 AAE values for MSOC were 5.62-6.95 for BB smoke and 8.46-10.0 for CC smoke. It was 318 obvious that the AAE value of BB MSOC was comparable to that of urban aerosols (average 319 7.10 \pm 0.45) in Beijing (Cheng et al., 2016) and the reported value (5.0–6.5) for urban 320 aerosols in India (Mukherjee et al., 2020), but the AAE values of CC MSOC were likely 321 higher than those for urban aerosols. It is obvious that CC-derived BrC fractions (WSOC, 322 HULIS-C, and MSOC) generally have relatively higher AAE values than ambient BrC, 323 thereby suggesting that the contribution of CC may improve the AAE values of BrC in the 324 325 atmosphere and should not be ignored.

As shown in Figures 2a and c, the average AAE values of the WSOC, HULIS-C, and 326 MSOC fractions in BB smoke were all lower than those for the same BrC fraction in CC 327 328 smoke, indicating that BB-derived BrC had a weaker wavelength dependence than CC-derived BrC. This finding agreed with the results reported in a previous study (Fan et al., 329 2016). The AAE values of the BrC fraction also varied according to the type of BrC fraction. 330 HULIS-C had the highest AAE values, which were slightly higher than those for WSOC but 331 much higher than those for MSOC (Figures 2a and 2c), indicating that water-soluble BrC 332 fractions had a greater wavelength dependency than the corresponding MSOC. This was 333 similar to the results of previous studies that found higher AAE values for WSOC than 334 MSOC in ambient aerosols (Cheng et al., 2016; Kim et al., 2016) and can be explained by the 335 fact that the strongly light-absorbing organic molecules are generally comprised of aromatic 336 337 structures with a high degree of conjugation and low solubility in water.

338 MAE₃₆₅ is an important parameter that characterizes the light absorption ability of

atmospheric BrC. As shown in Figures 2b and d, the MAE₃₆₅ values of WSOC and HULIS-C 339 were 0.9–1.5 (mean 1.2 \pm 0.3) and 1.1–1.6 (mean 1.3 \pm 0.2) m²/gC, respectively, for BB 340 smoke and 0.2–0.8 (mean 0.3 \pm 0.2) and 0.3–1.1 (mean 0.4 \pm 0.3) m²/gC, respectively, for CC 341 smoke. As the hydrophobic fraction of WSOC, the MAE₃₆₅ values of HULIS-C in BB and CC 342 smoke were slightly higher than that of the corresponding WSOC, suggesting that HULIS-C 343 had a stronger light absorbing ability. Moreover, the MAE₃₆₅ values of WSOC and HULIS-C 344 in BB smoke were comparable with the results of previous studies of the WSOC and 345 HULIS-C fractions in combustion-released smokes and ambient aerosols. For example, the 346 reported MAE₃₆₅ values of WSOC and HULIS-C were 0.8–1.6 and 1.0–1.5 m^2/gC , 347 respectively, in BB smoke PM_{2.5} (Park and Yu, 2016; Huo et al., 2018); 0.3–1.0 and 0.5–1.4 348 m^2/gC , respectively, in CC smoke particles (Li et al., 2018); and 0.1–1.5 m^2/gC in ambient 349 aerosols (Cheng et al., 2016; Yan et al., 2015; Zou et al., 2020). In contrast, the MAE₃₆₅ 350 values for MSOC were 1.9-2.7 m²/gC for BB smoke and 1.0-2.7 m²/gC for CC smoke, 351 which were 1.3-8.5 times higher than the corresponding values for HULIS-C and WSOC and 352 suggest that MSOC had the strongest light absorption capacity. The MAE₃₆₅ values of BB and 353 CC MSOC were comparable to the MAE₃₆₅ values of urban aerosols in Beijing winter 354 (average 1.45 \pm 0.26 m²/gC) (Yan et al., 2015) and the water-insoluble BrC (0.85–2.45 m²/gC) 355 in summer and winter ambient aerosols in Xi'an, Northwest China (Li et al., 2020b). 356 However, the values were higher than the MAE₃₆₅ value of aerosol MSOC in the Central 357 Tibetan Plateau (0.27–0.86 m^2/gC) (Wu et al., 2020), which may be due to the relatively low 358 combustion source contribution in this region. 359

As shown in Figures 2b and d, some differences were observed among the BrC fractions.

WSOC, HULIS-C, and MSOC in BB smoke all had relatively higher MAE₃₆₅ values than the same BrC fractions from CC, which suggested that BrC components emitted from BB had a relatively higher light absorption ability than those from CC and may therefore have a higher radiative force (Alexander et al., 2008). This finding is important for accurately assessing the climate effects of BrC from different combustion sources.

366

367 3.3. Spectral EEM features and identification of PARAFAC components

368 **3.3.1. The EEM fluorescence properties**

369 Fluorescence spectroscopy is a highly sensitive analytical technique for the identification of the sources and types of fluorophores in natural organic matter. In recent decades, 370 fluorescence spectroscopy has been widely used to characterize the fluorophores of 371 372 atmospheric BrC in field and laboratory studies (Chen et al., 2017; Chen et al., 2016; Qin et al., 2018; Fan et al., 2020). The typical EEM spectra of WSOC, HULIS-C, and MSOC 373 fractions from BB and CC are shown in Figure S2. To avoid concentration effects, the 374 fluorescence spectra were normalized by the OC content of WSOC, HULIS-C, and MSOC; 375 and the specific fluorescence intensities (a.u. L/(gC)) are shown. 376

In general, the different regions in the fluorescence spectra can be associated with organic fractions with different chemical characteristics (Table S1) (Chen et al., 2003; Cui et al., 2016; Qin et al., 2018). As shown in Figure S2, the EEM spectra were divided into five regions: protein-like amino acid (I), protein-like UV region (II, peak T_1), fulvic-like (III), tryptophan-like or microbial byproducts (IV, peak T_2), and humic-like (V) fluorophores (Qin et al., 2018; Cui et al., 2016; Chen et al., 2016). It was observed that the WSOC and

HULIS-C fractions exhibited two types of fluorescence peaks at $\lambda_{ex}/\lambda_{em} \approx (220-240)/(350-$ 383 390) nm (peak T₁) and $\lambda_{ex}/\lambda_{em} \approx (260-300)/(240-380)$ nm (peak T₂) (as marked in Figure S2), 384 which were mainly located in regions II and IV, respectively. These bands in the same range 385 as peaks T1 and T2 have previously been identified in the EEM fluorescence spectra of 386 water-soluble organic matter from rainwater/fog water (Santos et al., 2009; Santos et al., 2012) 387 and PM_{2.5} in an industrial city in Northwest China (Qin et al., 2018). As shown in Figure S2, 388 the fluorescence peaks T₁ and/or T₂ were the dominant peaks for WSOC and HULIS-C in 389 BB- and CC-derived smoke samples, which were consistent with previous observations of the 390 391 WSOC and HULIS-C fractions from BB (Huo et al., 2018; Fan et al., 2020). In general, peak T₁ mainly corresponded to the protein-like UV region, with a minor contribution from 392 fulvic-like substances; whereas peak T₂ was assigned as tryptophan-like or microbial 393 394 byproduct fluorophores. However, as reported in recent studies, non-nitrogen-containing species, such as naphthalene and phenol-derived compounds, may also contribute to the 395 fluorophores with peak T₂ in atmospheric aerosols (Chen et al., 2017, 2020). In addition, the 396 397 intensity of peak T₁ for BB- and CC-derived HULIS-C fractions was clearly stronger than the peak in ambient HULIS described in previous studies (Chen et al., 2017; Chen et al., 2016; 398 Fan et al., 2020; Qin et al., 2018), indicating that these BB- and CC-derived HULIS-C might 399 consist of more protein-like and/or aromatic amino acids than atmospheric HULIS. 400 However, these protein-like fluorescence peaks were observed to gradually decrease during 401 the aging process (e.g., hydroxyl radicals or ozone oxidation) in previous studies (Fan et al., 402 2019, 2020). This implied that most protein-like fluorophores in BB or CC BrC fractions may 403 have high reactivity. 404

As shown in Figure S2, the EEM spectra of the three MSOC fractions from crop straw 405 burning all had a strong fluorescence peak at long emission wavelengths ($E_X = 205-280$ nm, 406 407 $E_M = 360-380$ nm), which were located in regions V and IV and were generally assigned to humic-like fluorophores (Qin et al., 2018) or less oxygenated humic-like species (Chen et al., 408 2017; Chen et al., 2016). This peak was very weak or unobservable in the EEM fluorescence 409 spectra of the WSOC and HULIS-C fractions, suggesting that the higher intensity of the 410 fluorescence peak was mainly due to water-insoluble organic compounds with a high degree 411 of conjugation and/or aromaticity. As shown in Figure S2, unlike the EEM spectra of crop 412 413 straw MSOC, the EEM spectra of the three types of wood branches all displayed two obvious fluorescence peaks (e.g., peaks T_1 and T_2). These differences in the EEM spectra between 414 crop straw and wood burning-derived MSOC might be attributed to their molecular 415 416 differences, which should be investigated in future studies. The EEM spectra of the four bituminous coal smoke MSOC fractions displayed a similar fluorescence peak T₂ in the EEM 417 spectra, but only a strong peak T_1 was observed in the anthracite coal smoke MSOC. These 418 differences indicate that the fluorophores of MSOC were significantly influenced by the type 419 of fuel. 420

421

422 **3.3.2. Identification of PARAFAC components**

PARAFAC analysis further determined the fluorescent components of the water-soluble BrC fraction (WSOC and HULIS-C) and MSOC. As shown in Figure 3a, WSOC and HULIS-C generally contained four types of fluorophores (C_W1-C_W4). Based on previous studies of BrC EEM in combustion aerosols and ambient aerosols (Chen et al., 2017; Chen et

al., 2016; Huo et al., 2018; Qin et al., 2018), these four fluorophores could be assigned to two 427 protein-like substances (C_W1 and C_W2), one polyphenol-like component (C_W3), and one 428 humic-like compound (C_W4). The E_x/E_m maximum of C_W1 was located at 230/365 nm in 429 region II and was confirmed to be protein-like UV fluorophores. C_W2 ($E_X = 270$ nm, $E_M =$ 430 350 nm) was placed in region IV and was determined to be tryptophan-like or microbial 431 byproduct compounds (Chen et al., 2016; Li et al., 2020a), which have been identified in 432 aerosol WSOM (Chen et al., 2016; Matos et al., 2015) and BB-derived primary and secondary 433 WSOM (Huo et al., 2018). C_W3 ($E_X = 205/275$ nm, $E_M = 330$ nm) was located in regions I 434 435 and IV and had the characteristics of aromatic protein-like fluorophores or polyphenol-like components, most likely representing the fluorescence properties of polyphenol-like 436 components or compounds containing phenoxy groups (Mostofa et al., 2011). C_W4 (E_x = 437 438 215–320 nm, $E_M = 415$ nm) was located in the area where regions III and V overlap. These overlapping peaks were assigned to strong humic-like species fluorescence with an excitation 439 wavelength = 245 nm and two weaker shoulder peaks (Chen et al., 2016; Li et al., 2020a; Qin 440 et al., 2018; Huo et al., 2018; Fan et al., 2020); therefore, C_w4 was associated with typical 441 humic-like fluorophores. In summary, the fluorescence components identified in the WSOC 442 and HULIS-C fractions suggested that protein-like and humic-like substances were the two 443 major backbone components in water-soluble BrC fractions. 444

As shown in Figure 3b, four independent fluorescence components were also identified by PARAFAC analysis of MSOC (C_M1-C_M4). These components were similar to those of WSOC and HULIS-C, especially the positioning of the main peaks of the four fluorescent fluorophores. However, some small differences for component 2 (C_W2 and C_M2) and component 4 (C_W4 and C_M4) fluorophores were also observed. Unlike C_W2 in WSOC and HULIS-C, C_M2 in MSOC had its Ex/Em maximum at 285/360 nm, which was assigned to tryptophan-like compounds (Fan et al., 2020; Qin et al., 2018). In addition, two lower intensities of peaks at a lower excitation wavelength were also detected. The position of this fluorescence was closer to that of the typical tryptophan-like chromophores in aquatic DOM (Murphy et al., 2010). C_M4 in MSOC had a strong peak (EX = 255 nm, EM = 295 nm) but without the shoulder peaks observed for C_W4 in WSOC (Chen et al., 2016; Hou et al., 2018).

The relative contributions of individual chromophores identified by PARAFAC analysis 456 were calculated to express the relative contribution of each independent chromophore to the 457 overall fluorescence properties and are shown in Figure 4. The protein-like fluorescence 458 group (components 1 and 2), which were located at low emission wavelengths, dominated the 459 460 fluorophores of the BrC fractions in most BB and CC smoke samples. As shown in Figure 4, the contributions of protein-like substances in WSOC, HULIS-C, and MSOC were 47%-80%, 461 44%-87%, and 42%-70% (except CS MSOC), respectively, which were higher than the 462 463 contributions of polyphenol-like or humic-like substances in the same BrC fraction. These results are similar to the results reported for BrC from biomass combustion emissions in 464 previous studies (Huo et al., 2018; Fan et al., 2020). However, they were significantly 465 different from the EEM-PARAFAC properties of BrC in ambient aerosols, in which 466 component 4 was the most abundant chromophore (Chen et al., 2016; Li et al., 2020a). 467 However, component 4 accounted for only 13%-33% (except CS MSOC) and 3.8%-31% of 468 the BB and CC BrC fluorescence intensities, respectively, which were significantly lower 469 than those reported previously in ambient aerosols (30%-38%) (Li et al., 2020a). Moreover, 470

the contribution of polyphenol-like chromophores was 4.0%-39% and was comparable to that 471 of ambient aerosols (18%-26%) (Li et al., 2020a; Chen et al., 2016). It is obvious that the 472 four fluorescent components were all detected in the BrC fractions in combustion-derived 473 smokes and atmospheric aerosols; however, the protein-like compounds were the dominant 474 fluorophores in combustion-derived BrC whereas a relatively higher content of humic-like 475 fluorophores was identified in ambient aerosol BrC. These differences may be due to the 476 influence of various sources and atmospheric chemical processes on fluorophores (Li et al., 477 2020a; Fan et al., 2020). 478

Furthermore, some differences were also observed among the BrC fractions derived from different sources. As shown in Figure 4, the water-soluble BrC (WSOC and HULIS-C) from wood burning had a relatively higher content of component 3 than the water-soluble BrC from crop straw burning, which may be associated with the relatively large amount of lignin components in wood materials. In addition, even though their maturity was very different, there was no regular trend in the relative content of the fluorescent groups.

485

486 **3.4.** ¹H-NMR spectroscopy

¹H-NMR is an important analytical tool for the investigation of the functional groups of WSOC and HULIS in rural/urban aerosols (Fan et al., 2016; Zou et al., 2020) and rainwater (Santos et al., 2009; Santos et al., 2012). The typical ¹H-NMR spectra of the WSOC, HULIS-C, and MSOC fractions in smoke emitted from BB crop straw (e.g., WS) and CC (e.g., B-1) are shown in Figure 5, and the ¹H-NMR spectra of other BB and CC BrC fractions are shown in Figure S3. These BrC fractions had ¹H-NMR spectra similar to those derived from atmospheric HULIS and/or WSOC in rainwater (Santos et al., 2009; Santos et al., 2012),
BB aerosols (Fan et al., 2016), and ambient aerosols in urban and rural regions (Zou et al.,
2020).

As shown in Figure 5, the ¹H-NMR spectra were mainly composed of several distinct 496 sharp peaks superimposed on an unresolved broad band. According to previous studies and 497 reference NMR spectra (Zou et al., 2020; Chalbot et al., 2014; Chalbot et al., 2016), these 498 sharp peaks can be ascribed to low molecular weight organic compounds, such as 499 levoglucosan (\$3.52, \$3.67, \$4.08, and \$5.45 ppm), glucose (\$3.88-\$3.91 and \$3.81-\$3.85 500 ppm), and fructose ($\delta 3.79 - \delta 3.84$ ppm) associated with BB emissions; phthalic acid ($\delta 7.45 -$ 501 $\delta7.47$ and $\delta7.58$ ppm) and terephthalic acid ($\delta8.01$ ppm) associated with anthropogenic 502 activity; and the CH₃ in trimethylamine ($\delta 2.71$ and $\delta 2.89$ ppm), dimethylamine ($\delta 2.72$ ppm), 503 504 and monomethylamine ($\delta 2.55$ ppm) coemitted with ammonia. The relatively few and/or weak sharp peaks in the ¹H-NMR spectra of HULIS-C compared with those of WSOC may be the 505 result of low molecular weight organic compounds that have been removed from HULIS-C 506 through SPE isolation. In addition, all BB-derived WSOC had a high intensity of sharp peaks 507 associated with carbohydrates, such as levoglucosan, glucose, and fructose resonances, which 508 may be released from the thermal reactions of biopolymers, such as celluloses. As a 509 comparison, several peaks ($\delta 0.90$ and $\delta 1.35$ ppm) were observed in MSOC and were mainly 510 located in the aliphatic region. These peaks were weaker in WSOC and HULIS-C, suggesting 511 that more less polar aliphatic compounds were present in the MSOC fraction. 512

513 Despite some sharp peaks being identified, most of the signals in the ¹H-NMR spectra of 514 the BrC fractions presented a continuous unresolved distribution, suggesting that BrC consists

515	of a complex mixture of organic substances (Fan et al., 2016; Chalbot et al., 2014; Chalbot et
516	al., 2016). As shown in Figure 5, the functional groups of smoke BrC could be divided into
517	four representative categories: (1) R-H: aliphatic protons in alkyl chains (0.6-1.9 ppm),
518	including methyl (R-CH ₃) protons, methylene (R-CH ₂) protons, and methyne (R-CH) protons;
519	(2) H-C-C=: aliphatic protons bound to carbon atoms adjacent to unsaturated groups (1.9–3.2
520	ppm), including carbonyl (H-C-C=O) and imino (H-C-C=N) groups or aromatic rings; (3)
521	H-C-O: protons bound to oxygenated aliphatic carbons atoms in alcohols, polyols, ethers, and
522	esters (3.4-4.4 ppm), generally indicating that carbohydrates and ethers were present in
523	organic matter; and (4) Ar-H: protons bound to aromatic carbon atoms (6.5-8.5 ppm) (Fan et
524	al., 2016; Zou et al., 2020). The distribution of the four types of protons was obtained by
525	integrating the area of the observed ¹ H-NMR bands for each sample and is shown in Table 2.
526	These functional groups were also observed in the ¹ H-NMR spectra of HULIS in ambient
527	aerosols. In general, HULIS in ambient aerosols (Chalbot et al., 2014; Chalbot et al., 2016)
528	and rainwater (Santos et al., 2012) were characterized by the predominance of H-C (41%-
529	60%), moderate contents of H-C-C= (25%-34%) and H-C-O (4.0%-49%), and a lesser
530	contribution of Ar-H (2.0%–6.0%). However, it was obvious that the relative content of Ar–H
531	groups (18%-37%) in HULIS-C from both combustion processes (BB and CC) was higher
532	than the levels in ambient HULIS (Table 2), which suggests that BB- and CC-derived
533	HULIS-C contained more aromatic structures than ambient HULIS. This was consistent with
534	reports that more aromatic structures are observed in HULIS in colder season aerosol
535	particles in northern China, which may be related to the amount of residential coal and straw
536	combustion (Li et al., 2018; Sun et al., 2017).

As shown in Table 2, the relative contents of the four functional groups (i.e., R-H, 537 H-C-C=, H-C-O, and Ar-H) varied with the type of BrC. For example, BB WSOC was always 538 characterized by a relatively high level of oxygenated H-C-O groups and a relatively low 539 level of aliphatic R-H groups compared with the corresponding MSOC extracted with 540 methanol. As shown in Figure 5, several strong signals in aliphatic R-H were also identified 541 in MSOC, but they were weaker in the WSOC fraction. This was considered reasonable 542 because the less polar aliphatic compounds were difficult to dissolve in water but could be 543 extracted by methanol. As the hydrophobic fraction of WSOC, HULIS-C contained a 544 545 relatively higher content of the Ar-H group and a relatively lower content of the oxygenated H-C-O group than the original WSOC for all BB and CC smoke samples. This was due to 546 most of the low molecular oxygenated compounds not being retained by the 547 548 hydrophilic-lipophilic balance cartridges and the enrichment of aromatic species (Fan et al., 2016; Zou et al., 2020). 549

Some distinct differences in the distribution of functional groups were also observed 550 among the BrC fractions from BB and CC. As shown in Figure 5, several oxygenated 551 compounds (e.g., levoglucosan) were identified, with higher intensity signals in the BB 552 WSOC fraction, but they were weaker in the WSOC fraction from CC. The relative content of 553 the H-C-O group was in the range of 34%–54% for the six BB WSOCs, which was higher 554 than the values (9.0–34%) for the five CC WSOCs. These oxygenated aliphatic compounds 555 were mainly assigned to carbohydrates and polyols that may be caused by the degradation of 556 biomass polymers such as cellulose (Fan et al., 2012; Fan et al., 2016; Lin et al., 2016). In 557 contrast, the BrC fractions from CC indicated a relatively higher level of unsaturated 558

559	functional groups (Table 2). For example, there was a relatively higher content of Ar-H
560	(30%-37%) and H-C-C= $(34%-40%)$ in the smoke HULIS-C from CC than from BB,
561	indicating that CC HULIS-C contained more unsaturated structures, such as aromatic
562	structures and unsaturated aliphatics (Wu et al., 2014; Dong et al., 2021; Huang et al., 2020).

563

564 **3.5 Oxidative potential**

The oxidative potential of the BB- and CC-derived BrC fractions (i.e., WSOC, HULIS-C, 565 and MSOC) was investigated through a DTT assay, and the results are shown in Table S2 and 566 Figure 6. The DTT_m value of WSOC ranged from 0.5 pmol/min/µg (B-3) to 7.4 pmol/min/µg 567 (CS) with a mean of 3.8 pmol/min/ μ g. These DTT_m values are comparable with those for the 568 water soluble fractions of BB, CC, and diesel soot $(1.4 \pm 0.6, 2.1 \pm 2.3 \text{ and } 1.1 \pm 0.4 \text{ pmol/min/}\mu\text{g})$ 569 570 (Li et al., 2019; Zhu et al., 2019) but were much lower than the ranges of 14–25 pmol/min/µg in Los Angeles wildfire aerosol samples, 22-68 pmol/min/µg in Atlanta PM_{2.5} samples, and 571 0.13±0.10 nmol/min/µg in Beijing PM_{2.5} samples (Verma et al., 2012; Bates et al., 2019, Yu et 572 573 al., 2019). These results suggested that the water-soluble fraction from BB and CC in this study had a weaker ROS generation capacity than ambient aerosols, which was likely due to 574 the differences in the chemical composition of water-soluble fractions in BB and CC smoke 575 particles and ambient aerosols (Lin and Yu, 2011; Dou et al., 2015; Wong et al., 2019; Lin and 576 577 Yu, 2019). In general, ambient aerosols contain various sources; and the contribution of other sources, such as vehicle emissions or anthropogenic emissions, and transition metals (e.g., Fe, 578 Cu) could increase the ability of atmospheric water-soluble fractions to produce ROS species 579 (Ma et al., 2018; Li et al., 2019). In addition, because of the evaporative loss of non- or 580

581

582

less-DTT active semivolatile organic compounds, the DTT activities of BB-derived water-soluble fractions were enhanced during the aging process (Wong et al., 2019).

The DTT_m values of BB- and CC-derived HULIS-C ranged from 0.5 pmol/min/µg (B-3) 583 to 5.5 pmol/min/µg (RS) with a mean of 2.3 pmol/min/µg. These values were lower than the 584 range (15–45 pmol/min/µg) previously reported for ambient HULIS measured with the same 585 DTT assay (Lin and Yu, 2011; Ma et al., 2018; Verma et al., 2012). As an important 586 component of WSOC, the DTT activity of HULIS-C accounted 63.1% ±15.5% (41.4%-90.6%) 587 for that of WSOC in the BB and CC samples. These values of DDT_{m.HULIS}/DTT_{m.WSOC} were 588 always higher than the organic carbon contribution of HULIS-C to WSOC for the same 589 sample (Table 1), therefore indicating that hydrophobic HULIS-C was an important 590 redox-active fraction in the BB- and CC-derived WSOC compounds. This result was 591 592 comparable with the higher oxidative contribution (64%) of HULIS-C following water extracts from ambient aerosols in Atlanta (Verma et al., 2012). As reviewed by Win et al. 593 (2018), this phenomenon can be explained by the specific organic species and functional 594 groups with DTT activity in HULIS-C. As described in previous studies and in this study, the 595 hydrophobic organic fractions isolated by the SPE column are mainly comprised of aromatic 596 compounds (Sannigrahi et al., 2006; Fan et al., 2016; Huo et al., 2018). These compounds 597 most likely include some of the redox-active species such as nitro-PAHs and quinones (Verma 598 et al., 2012), which can catalyze the oxidation of cellular antioxidants and generate ROS 599 species (Verma et al., 2012; Lin and Yu, 2011). In addition, as the charge transfer intermediate, 600 601 the reversible redox sites in HULIS lead to continuous ROS production (Ma et al., 2018; Lin and Yu, 2011). 602

603	The DTT _m values of MSOC were in the range of 3.1 pmol/min/ μ g (B-4) to 84
604	pmol/min/ μg (RS). These values were comparable to those reported in previous studies
605	involving atmospheric aerosol methanol extracts (~55 pmol/min/ μ g) (Verma et al., 2012). As
606	shown in Figure 6, the \mbox{DTT}_m values of MSOC were much higher than those of WSOC and
607	HULIS-C from the same smoke samples, which suggested that the water-insoluble
608	components possessed significant oxidative properties that are relevant in toxicological
609	studies (Verma et al., 2012). These results were consistent with the results of previous studies
610	showing that water-insoluble compounds made the largest contribution to the oxidative
611	potential (Verma et al., 2012; Verma et al., 2015).

The DTT_m values of the BrC fractions varied with the type of fuel. As shown in Table S2, 612 the DTT_m values of BB WSOC were 4.5–7.4 pmol/min/µg, which was significantly higher 613 614 than the range of 0.5–2.1 pmol/min/µg for CC WSOC. Similar results were also observed for the HULIS and MSOC fractions (Figure 6). These results indicated that the BrC fractions 615 from BB had higher oxidative potential values than those from CC and therefore more readily 616 617 catalyzed the generation of ROS. Furthermore, no regular variations were observed for the oxidative potential of water-soluble BrC (e.g., WSOC and HULIS-C) in BB or CC smoke 618 samples, but the MSOC in crop straw smoke had a much higher DTT_{mass} value than the 619 MSOC in smoke samples from wood burning and CC. These differences were associated with 620 the differences in the amounts of redox-active compounds in each BrC fraction. There is a 621 need for more studies to investigate the relationship between the molecular structures in BB 622 623 smoke BrC and their DTT activities.

625 **3.6** Correlation between oxidative potential and chemical compositions of BrCs

The BrCs produced by the BB and CC processes generally have different oxidative 626 potentials. The oxidative potential values of water-soluble BrC (WSOC and HULIS-C) were 627 much lower than those in MSOC, and the BB BrC fractions had higher oxidative potential 628 values than CC BrC fractions. These results suggested that BrC from different sources 629 exhibited distinct redox properties (Lin and Yu, 2011). To elucidate the association of 630 chemical characteristics with the oxidative potential of BB and CC, principal component 631 analysis (PCA) and Pearson correlation coefficients were conducted. Because the optical and 632 chemical properties were all obtained based on organic matter rather than PM, the oxidative 633 potential value normalized by the organic carbon mass (DTT_{OC}) of each fraction was used 634 here to present DTT activities, as well as the capacity to produce ROS species. In addition, 635 636 considering the statistical significance and quantity, the WSOC, HULIS-C and MSOC data were analyzed together. 637

The results are shown in Figure 7 and Table 3. It is obvious that DTT_{OC} showed a positive loading for both principal component 1 (PC1) and principal component 2 (PC2), and DTT_{OC} was grouped with fluorophores C4 and MAE₃₆₅. These results are also given by the Pearson correlation coefficient analysis in which the DTT_{OC} values showed significant positive correlations with the parameters MAE₃₆₅ (R=0.697, p<0.01) and C4 proportion (R=0.560, p<0.01). These results suggested that fluorophore C4 and high light-absorbing components may significantly contribute to the DDT activities of BrC compounds.

645 Moreover, a significant positive relationship was also observed for C4 and MAE₃₆₅ 646 (R=0.531, p<0.01), which indicated that C4 may be the main substance leading to the light

absorption of BrC. As reported previously, MAE₃₆₅ is related to the aromatic structure of the 647 conjugated system (Andrade-Eiroa et al., 2013, Fan et al., 2018), and fluorophore C4 was 648 considered to be a highly oxygenated species containing more carbonyl and carboxyl groups 649 (Chen et al., 2016, Li et al., 2020a). Therefore, the C4 component may mainly comprise 650 651 chemical species with a conjugated system and highly oxygenated species, such as quinones or aromatic acids, which were believed to be the key components for the enhancement of the 652 ability of BrC to produce ROS species (Lin and Yu, 2011, Jiang et al., 2016, Verma et al., 653 2012). These results also explained that the water-soluble BrC fractions in BB and CC smoke 654 655 showed relatively lower DTT consumption rate than those in ambient aerosols, in which distinctly higher contents of fluorophore C4 were observed in the water-soluble fraction 656 (Matos et al., 2015; Chen et al., 2016). 657

658 We note that a positive correlation was observed between DTT_{OC} and R-H and a negative correlation was observed between DTT_{OC} and Ar-H; however, it is scientifically 659 unreasonable. The main reason is that ¹H NMR spectroscopy only measures the 660 concentrations of nonexchangeable hydrogen functional groups in BrC compounds. Some 661 organic compounds not carrying nonexchangeable hydrogen atoms, such as carbonyl or 662 carboxylic groups in BrC, cannot be detected by ¹H NMR (Chalbot and Kavouras 2014; 663 Paglione et al., 2014). However, some of these oxygenated functional groups likely have the 664 ability to catalyze the generation of ROS species (Lin and Yu, 2011; Verma et al., 2015). In 665 addition, the H/C ratios of different hydrogen functional groups (i.e., R-H, H-C-C=, H-C-O, 666 and Ar-H) are very different; thus, the relative abundances of hydrogen functional groups are 667 difficult to compare with the carbon functional groups in BrC compounds (Decesari et al., 668

669 2007). Therefore, it is necessary that other NMR techniques such as solution-state 13 C NMR 670 and two-dimensional heteronuclear (1 H- 13 C) NMR be used to explore the chemical functional 671 groups associated with the oxidative potential of BrC in future studies.

672

673 **4. Conclusions**

In this study, the primary BrC fractions (i.e., WSOC, HULIS-C, and MSOC) emitted 674 from BB and CC were comprehensively investigated to determine their content, light 675 absorption, fluorophores, chemical properties, and oxidative potential. The results indicated 676 that both BB and CC were important sources of atmospheric BrC. It was found that BB 677 generated more of the water-soluble BrC fraction whereas CC released more of the 678 methanol-soluble BrC fraction in smoke PM25. The results also enhanced our understanding 679 680 of the optical characteristics, chemical composition, and oxidative potential of the water- and methanol-soluble BrC fractions. The MSOC fraction had higher MAE₃₆₅ values than 681 HULIS-C and WSOC, suggesting that water-insoluble BrC possessed a stronger light 682 absorbing capacity. In addition, BB BrC generally had higher MAE₃₆₅ and lower AAE values 683 than the corresponding CC BrC fractions, suggesting that the former had a higher light 684 absorption capacity and weaker wavelength dependence. The EEM-PARAFAC analysis 685 identified two protein-like compounds, one polyphenol-like component, and one humic-like 686 compound for all BrC fractions, among which the protein-like compounds were the dominant 687 components. The ¹H NMR analysis showed that the BB and CC BrC fractions contained R-H, 688 H-C-C=, H-C-O, and Ar-H groups, among which WSOC and HULIS-C were always 689 characterized by more oxygenated H-C-O groups and fewer aliphatic R-H groups than MSOC. 690

In addition, water-soluble BB BrC contained more highly oxygenated groups, suggesting that 691 they may have a stronger influence on the binding of metals by organic aerosols. Our study 692 also indicated that MSOC had higher DTT_m values than WSOC and HULIS-C, suggesting a 693 higher ROS generation capacity. In addition, relatively higher oxidative contribution 694 (63.1% ±15.5%) of HULIS-C in WSOC were observed for all BB and CC smoke samples, 695 highlighted that HULIS was a major contributor of ROS production in WSOC. The BB BrC 696 fractions generally had a higher oxidative potential than CC BrC, which may suggest that BB 697 BrC was more readily able to catalyze the generation of ROS and therefore lead to more 698 699 severe harm to human health. More importantly, the PCA and Pearson correlation analysis indicated that highly oxygenated humic-like fluorophore C4 may be an important DTT active 700 substance in BrC. 701

It should be noted that the BB and CC BrC fractions would experience a series of chemical reactions once they are emitted into the atmosphere, resulting in changes to their optical properties and DTT activities. Thus, future studies should focus on the chemical, optical, and oxidative potential characteristics of BrC during the aging processes with smoke particles in the tropospheric environment (Fan et al., 2020; Wong et al., 2019).

707

708 Data availability. The research data can be accessed upon request to the corresponding
709 author (<u>songjzh@gig.ac.cn</u>).

710

Author contributions. J. Song and P. Peng designed the research together. T. Cao, M. Li, and
C. Zou conducted the combustion experiments. T. Cao, M. Li, and C Yu extracted and

713	analyzed the BrC fractions. T. Cao and J. Song wrote the paper. X. Fan, J Wang, Z Yu, and P.
714	Peng commented on and revised the paper.

715

716 **Competing interests.** The authors declare that they have no conflicts of interest.

717

Acknowledgments. This study was supported by the National Natural Science Foundation of China (41977188 and 41673177), the State Key Laboratory of Organic Geochemistry, GIGCAS (SKLOG2020-3), and Guangdong Foundation for Program of Science and Technology Research (2019B121205006). We greatly appreciate the assistance of two anonymous reviewers for the helpful comments that greatly improved the quality of this manuscript.

724

725 **References**

Alexander, D. T. L., Crozier, P. A., and Anderson, J. R.: Brown carbon spheres in East Asian
outflow and their optical properties, Science, 321, 833-836, 10.1126/science.1155296,
2008.

Andrade-Eiroa, Á., Canle, M., and Cerdá, V.: Environmental Applications of
 Excitation-Emission Spectrofluorimetry: An In-Depth Review I, Applied Spectroscopy
 Reviews, 48, 1-49, 10.1080/05704928.2012.692104, 2013.

Andreae, M. O., and Gelencser, A.: Black carbon or brown carbon? The nature of
light-absorbing carbonaceous aerosols, Atmospheric Chemistry and Physics, 6,

734 3131-3148, DOI 10.5194/acp-6-3131-2006, 2006.

735	Atwi, K., Mondal, A., Pant, J., Cheng, Z., El Hajj, O., Ijeli, I., Handa, H., and Saleh, R.:
736	Physicochemical properties and cytotoxicity of brown carbon produced under different
737	combustion conditions, Atmospheric Environment, 244, 117881,
738	10.1016/j.atmosenv.2020.117881, 2021.
739	Bai, Z., Zhang, L., Cheng, Y., Zhang, W., Mao, J., Chen, H., Li, L., Wang, L., and Chen, J.:
740	Water/Methanol-Insoluble Brown Carbon Can Dominate Aerosol-Enhanced Light
741	Absorption in Port Cities, Environmental science & technology, 54, 14889-14898,
742	10.1021/acs.est.0c03844, 2020.
743	
744	Bates, J. T., Fang, T., Verma, V., Zeng, L., Weber, R. J., Tolbert, P. E., Abrams, J. Y., Sarnat, S.
745	E., Klein, M., Mulholland, J. A., and Russell, A. G.: Review of Acellular Assays of
746	Ambient Particulate Matter Oxidative Potential: Methods and Relationships with
747	Composition, Sources, and Health Effects, Environmental science & technology, 53,
748	4003-4019, 10.1021/acs.est.8b03430, 2019.

Chalbot, M. G., Brown, J., Chitranshi, P., da Costa, G. G., Pollock, E. D., and Kavouras, I. G.:
Functional characterization of the water-soluble organic carbon of size-fractionated
aerosol in the southern Mississippi Valley, Atmos Chem Phys, 14, 6075-6088,
10.5194/acp-14-6075-2014, 2014.

- Chalbot, M. C., and Kavouras, I. G.: Nuclear magnetic resonance spectroscopy for
 determining the functional content of organic aerosols: a review, Environmental
 pollution, 191, 232-249, 10.1016/j.envpol.2014.04.034, 2014.
- 756 Chalbot, M. G., Chitranshi, P., da Costa, G. G., Pollock, E., and Kavouras, I. G.:

757	Characterization of water-soluble organic matter in urban aerosol by (1)H-NMR
758	spectroscopy, Atmos Environ (1994), 128, 235-245, 10.1016/j.atmosenv.2015.12.067,
759	2016.
760	Chen, Q., Miyazaki, Y., Kawamura, K., Matsumoto, K., Coburn, S., Volkamer, R., Iwamoto,
761	Y., Kagami, S., Deng, Y., Ogawa, S., Ramasamy, S., Kato, S., Ida, A., Kajii, Y., and

762 Mochida, M.: Characterization of Chromophoric Water-Soluble Organic Matter in Urban,

Forest, and Marine Aerosols by HR-ToF-AMS Analysis and Excitation-Emission Matrix

764 Spectroscopy, Environmental science & technology, 50, 10351-10360,
765 10.1021/acs.est.6b01643, 2016.

- Chen, Q., Ikemori, F., Nakamura, Y., Vodicka, P., Kawamura, K., and Mochida, M.: Structural
 and Light-Absorption Characteristics of Complex Water-Insoluble Organic Mixtures in
 Urban Submicrometer Aerosols, Environmental science & technology, 51, 8293-8303,
 10.1021/acs.est.7b01630, 2017.
- Chen, Q., Wang, M., Wang, Y., Zhang, L., Li, Y., and Han, Y.: Oxidative Potential of
 Water-Soluble Matter Associated with Chromophoric Substances in PM2.5 over Xi'an,
 China, Environmental science & technology, 53, 8574-8584, 10.1021/acs.est.9b01976,
 2019.

Chen, Q., Li, J., Hua, X., Jiang, X., Mu, Z., Wang, M., Wang, J., Shan, M., Yang, X., Fan, X., 774 Song, J., Wang, Y., Guan, D., and Du, L.: Identification of species and sources of 775 atmospheric chromophores by fluorescence excitation-emission matrix with parallel 776 analysis, 777 factor The Science of the total environment, 718, 137322, 10.1016/j.scitotenv.2020.137322, 2020. 778

779	Chen, W., Westerhoff, P., Leenheer, J. A., and Booksh, K.: Fluorescence excitation - Emission
780	matrix regional integration to quantify spectra for dissolved organic matter,
781	Environmental science & technology, 37, 5701-5710, 10.1021/es034354c, 2003.
782	Chen, Y., and Bond, T. C.: Light absorption by organic carbon from wood combustion,
783	Atmospheric Chemistry and Physics, 10, 1773-1787, DOI 10.5194/acp-10-1773-2010,

2010. 784

Cheng, Y., He, K. B., Du, Z. Y., Engling, G., Liu, J. M., Ma, Y. L., Zheng, M., and Weber, R. 785

J.: The characteristics of brown carbon aerosol during winter in Beijing, Atmospheric 786

Environment, 127, 355-364, 10.1016/j.atmosenv.2015.12.035, 2016. 787

- Cui, X., Zhou, D., Fan, W., Huo, M., Crittenden, J. C., Yu, Z., Ju, P., and Wang, Y.: The 788 effectiveness of coagulation for water reclamation from a wastewater treatment plant 789 790 that has a long hydraulic and sludge retention times: A case study, Chemosphere, 157, 224-231, 10.1016/j.chemosphere.2016.05.009, 2016. 791
- Decesari, S., Mircea, M., Cavalli, F., Fuzzi, S., Moretti, F., Tagliavini, E., and Facchini, M. C.: 792 Source attribution of water-soluble organic aerosol by nuclear magnetic resonance 793 spectroscopy, Environmental science & technology, 41, 2479-2484, 10.1021/es0617111, 794 795 2007.
- Dong, Z., Jiang, N., Zhang, R., Xu, Q., Ying, Q., Li, Q., and Li, S.: Molecular characteristics, 796 source contributions, and exposure risks of polycyclic aromatic hydrocarbons in the core 797 city of Central Plains Economic Region, China: Insights from the variation of haze 798 The 799 levels, Science of the total environment, 757, 143885, 10.1016/j.scitotenv.2020.143885, 2021. 800

801	Dou, J., Lin, P., Kuang, B. Y., and Yu, J. Z.: Reactive Oxygen Species Production Mediated
802	by Humic-like Substances in Atmospheric Aerosols: Enhancement Effects by Pyridine,
803	Imidazole, and Their Derivatives, Environmental science & technology, 49, 6457-6465,
804	10.1021/es5059378, 2015.
805	Evangeliou, N., Kylling, A., Eckhardt, S., Myroniuk, V., Stebel, K., Paugam, R., Zibtsev, S.,
806	and Stohl, A.: Open fires in Greenland in summer 2017: transport, deposition and
807	radiative effects of BC, OC and BrC emissions, Atmospheric Chemistry and Physics, 19,

- 808 1393-1411, 10.5194/acp-19-1393-2019, 2019.
- Fan, X., Li, M., Cao, T., Cheng, C., Li, F., Xie, Y., Wei, S., Song, J., and Peng, P. a.: Optical
 properties and oxidative potential of water-and alkaline-soluble brown carbon in smoke
 particles emitted from laboratory simulated biomass burning, Atmospheric Environment,
 194, 48-57, 10.1016/j.atmosenv.2018.09.025, 2018.
- Fan, X., Yu, X., Wang, Y., Xiao, X., Li, F., Xie, Y., Wei, S., Song, J., and Peng, P. a.: The
 aging behaviors of chromophoric biomass burning brown carbon during dark aqueous
 hydroxyl radical oxidation processes in laboratory studies, Atmospheric Environment,
- 816 205, 9-18, 10.1016/j.atmosenv.2019.02.039, 2019.
- 817 Fan, X., Cao, T., Yu, X., Wang, Y., Xiao, X., Li, F., Xie, Y., Ji, W., Song, J., Peng, P., amp,
- apos, and an: The evolutionary behavior of chromophoric brown carbon during ozone
- aging of fine particles from biomass burning, Atmospheric Chemistry and Physics, 20,
- 820 4593-4605, 10.5194/acp-20-4593-2020, 2020.
- Fan, X. J., Song, J. Z., and Peng, P. A.: Comparison of isolation and quantification methods to
- measure humic-like substances (HULIS) in atmospheric particles, Atmospheric

Environment, 60, 366-374, 10.1016/j.atmosenv.2012.06.063, 2012.

- Fan, X. J., Wei, S. Y., Zhu, M. B., Song, J. Z., and Peng, P. A.: Comprehensive
 characterization of humic-like substances in smoke PM2.5 emitted from the combustion
 of biomass materials and fossil fuels, Atmospheric Chemistry and Physics, 16,
 13321-13340, 10.5194/acp-16-13321-2016, 2016.
- Gao, D., Mulholland, J. A., Russell, A. G., and Weber, R. J.: Characterization of
 water-insoluble oxidative potential of PM2.5 using the dithiothreitol assay, Atmospheric
 Environment, 224, 117327, 10.1016/j.atmosenv.2020.117327, 2020.
- Geng, C., Chen, J., Yang, X., Ren, L., Yin, B., Liu, X., and Bai, Z.: Emission factors of
 polycyclic aromatic hydrocarbons from domestic coal combustion in China, Journal of
 environmental sciences, 26, 160-166, 10.1016/s1001-0742(13)60393-9, 2014.
- Hakimzadeh, M., Soleimanian, E., Mousavi, A., Borgini, A., De Marco, C., Ruprecht, A. A.,
- and Sioutas, C.: The impact of biomass burning on the oxidative potential of PM2.5 in
- the metropolitan area of Milan, Atmospheric Environment, 224, 117328,
 10.1016/j.atmosenv.2020.117328, 2020.
- He, W., and Hur, J.: Conservative behavior of fluorescence EEM-PARAFAC components in
 resin fractionation processes and its applicability for characterizing dissolved organic
 matter, Water research, 83, 217-226, 10.1016/j.watres.2015.06.044, 2015.
- Hoffer, A., Gelencser, A., Guyon, P., Kiss, G., Schmid, O., Frank, G. P., Artaxo, P., and
 Andreae, M. O.: Optical properties of humic-like substances (HULIS) in
 biomass-burning aerosols, Atmospheric Chemistry and Physics, 6, 3563-3570, DOI
 10.5194/acp-6-3563-2006, 2006.

845	Hou, C., Shao, L., Hu, W., Zhang, D., Zhao, C., Xing, J., Huang, X., and Hu, M.:
846	Characteristics and aging of traffic-derived particles in a highway tunnel at a coastal city
847	in southern China, The Science of the total environment, 619-620, 1385-1393.
848	10.1016/j.scitotenv.2017.11.165, 2018.

- 849 Huang, R. J., Yang, L., Shen, J., Yuan, W., Gong, Y., Guo, J., Cao, W., Duan, J., Ni, H., Zhu,
- 850 C., Dai, W., Li, Y., Chen, Y., Chen, Q., Wu, Y., Zhang, R., Dusek, U., O'Dowd, C., and
- Hoffmann, T.: Water-Insoluble Organics Dominate Brown Carbon in Wintertime Urban
- Aerosol of China: Chemical Characteristics and Optical Properties, Environmental
 science & technology, 54, 7836-7847, 10.1021/acs.est.0c01149, 2020.
- Huo, Y. Q., Li, M., Jiang, M. H., and Qi, W. M.: Light absorption properties of HULIS in
 primary particulate matter produced by crop straw combustion under different moisture
 contents and stacking modes, Atmospheric Environment, 191, 490-499,
 10.1016/j.atmosenv.2018.08.038, 2018.
- Izhar, S., Gupta, T., and Panday, A. K.: Improved method to apportion optical absorption by
 black and brown carbon under the influence of haze and fog at Lumbini, Nepal, on the
 Indo-Gangetic Plains, Environmental pollution, 263, 114640,
 10.1016/j.envpol.2020.114640, 2020.
- Jiang, H., Jang, M., Sabo-Attwood, T., and Robinson, S. E.: Oxidative potential of secondary
 organic aerosols produced from photooxidation of different hydrocarbons using outdoor
 chamber under ambient sunlight, Atmospheric Environment, 131, 382-389,
 10.1016/j.atmosenv.2016.02.016, 2016.
- Kim, H., Kim, J. Y., Jin, H. C., Lee, J. Y., and Lee, S. P.: Seasonal variations in the 40

867	light-absorbing properties of water-soluble and insoluble organic aerosols in Seoul,
868	Korea, Atmospheric Environment, 129, 234-242, 10.1016/j.atmosenv.2016.01.042, 2016.
869	Kramer, A. J., Rattanavaraha, W., Zhang, Z., Gold, A., Surratt, J. D., and Lin, YH.: Assessing
870	the oxidative potential of isoprene-derived epoxides and secondary organic aerosol,
871	Atmospheric Environment, 130, 211-218, 10.1016/j.atmosenv.2015.10.018, 2016.
872	Kumar, N. K., Corbin, J. C., Bruns, E. A., Massabo, D., Slowik, J. G., Drinovec, L., Mocnik,
873	G., Prati, P., Vlachou, A., Baltensperger, U., Gysel, M., El-Haddad, I., and Prevot, A. S.
874	H.: Production of particulate brown carbon during atmospheric aging of residential
875	wood-burning emissions, Atmospheric Chemistry and Physics, 18, 17843-17861,
876	10.5194/acp-18-17843-2018, 2018a.
877	Kumar, V., Rajput, P., and Goel, A.: Atmospheric abundance of HULIS during wintertime in
878	Indo-Gangetic Plain: impact of biomass burning emissions, Journal of Atmospheric
879	Chemistry, 75, 385-398, 10.1007/s10874-018-9381-4, 2018b.
880	Laskin, A., Laskin, J., and Nizkorodov, S. A.: Chemistry of atmospheric brown carbon,
881	Chemical reviews, 115, 4335-4382, 10.1021/cr5006167, 2015.
882	Lawaetz, A. J., and Stedmon, C. A.: Fluorescence Intensity Calibration Using the Raman
883	Scatter Peak of Water, Applied Spectroscopy, 63, 936-940,
884	10.1366/000370209788964548, 2009.
885	Li, J., Chen, Q., Hua, X., Chang, T., and Wang, Y.: Occurrence and sources of chromophoric
886	organic carbon in fine particulate matter over Xi'an, China, The Science of the total
887	environment, 725, 138290, 10.1016/j.scitotenv.2020.138290, 2020a.

Li, J., Zhang, Q., Wang, G., Li, J., Wu, C., Liu, L., Wang, J., Jiang, W., Li, L., Ho, K. F., and

- Cao, J.: Optical properties and molecular compositions of water-soluble and
 water-insoluble brown carbon (BrC) aerosols in northwest China, Atmospheric
 Chemistry and Physics, 20, 4889-4904, 10.5194/acp-20-4889-2020, 2020b.
- Li, M., Fan, X., Zhu, M., Zou, C., Song, J., Wei, S., Jia, W., and Peng, P.: Abundances and
- light absorption properties of brown carbon emitted from residential coal combustion in
 China, Environmental science & technology, 10.1021/acs.est.8b05630, 2019.
- Li, R., Han, Y., Wang, L., Shang, Y., and Chen, Y.: Differences in oxidative potential of black
 carbon from three combustion emission sources in China, Journal of environmental
 management, 240, 57-65, 10.1016/j.jenvman.2019.03.070, 2019.
- Li, X., Han, J., Hopke, P. K., Hu, J., Shu, Q., Chang, Q., and Ying, Q.: Quantifying primary
 and secondary humic-like substances in urban aerosol based on emission source
 characterization and a source-oriented air quality model, Atmospheric Chemistry and
 Physics, 19, 2327-2341, 10.5194/acp-19-2327-2019, 2019.
- Lin, M., and Yu, J. Z.: Dithiothreitol (DTT) concentration effect and its implications on the
 applicability of DTT assay to evaluate the oxidative potential of atmospheric aerosol
 samples, Environmental pollution, 251, 938-944, 10.1016/j.envpol.2019.05.074, 2019.
- Lin, P., and Yu, J. Z.: Generation of reactive oxygen species mediated by humic-like
 substances in atmospheric aerosols, Environmental science & technology, 45,
 10362-10368, 10.1021/es2028229, 2011.
- Lin, P., Laskin, J., Nizkorodov, S. A., and Laskin, A.: Revealing Brown Carbon
 Chromophores Produced in Reactions of Methylglyoxal with Ammonium Sulfate,
- 910 Environmental science & technology, 49, 14257-14266, 10.1021/acs.est.5b03608, 2015.

911	Lin.	Р	Aiona.	P.	K.,	Li.	Y	Shiraiwa.	M.,	Laskin.	J.,	Nizkorodov	. S.	A.,	and	Laskin.	A.:
J T T	D 111,	±.,	i iioiia,	••	,	,	±.,	Dim ai way	, ITI .,	Laonin,	•••,	1 (ILROIOGO)	,	,	unu	Luomi,	1 1

- Molecular Characterization of Brown Carbon in Biomass Burning Aerosol Particles,
 Environmental science & technology, 50, 11815-11824, 10.1021/acs.est.6b03024, 2016.
- Ma, Y., Cheng, Y., Qiu, X., Cao, G., Fang, Y., Wang, J., Zhu, T., Yu, J., and Hu, D.: Sources
 and oxidative potential of water-soluble humic-like substances (HULIS_{WS}) in fine
 particulate matter (PM_{2.5}) in Beijing, Atmospheric Chemistry and Physics, 18,
 5607-5617, 10.5194/acp-18-5607-2018, 2018.
- 918 Matos, J. T. V., Freire, S. M. S. C., Duarte, R. M. B. O., and Duarte, A. C.: Natural organic
- matter in urban aerosols: Comparison between water and alkaline soluble components
 using excitation-emission matrix fluorescence spectroscopy and multiway data analysis,
 Atmospheric Environment, 102, 1-10, 10.1016/j.atmosenv.2014.11.042, 2015.
- 922 Mostofa, K. M. G., Wu, F. C., Liu, C. Q., Vione, D., Yoshioka, T., Sakugawa, H., and Tanoue,
- E.: Photochemical, microbial and metal complexation behavior of fluorescent dissolved
 organic matter in the aquatic environments, Geochem. J., 45, 235-254, 2011.
- 925 Moufarrej, L., Courcot, D., and Ledoux, F.: Assessment of the PM2.5 oxidative potential in a
- 926 coastal industrial city in Northern France: Relationships with chemical composition,
- 927 local emissions and long range sources, The Science of the total environment, 748,
- 928 141448, 10.1016/j.scitotenv.2020.141448, 2020.
- Mukherjee, A., Dey, S., Rana, A., Jia, S., Banerjee, S., and Sarkar, S.: Sources and
 atmospheric processing of brown carbon and HULIS in the Indo-Gangetic Plain: Insights
 from compositional analysis, Environmental pollution, 267, 115440,
 10.1016/j.envpol.2020.115440, 2020.

933	Murphy, K. R., Butler, K. D., Spencer, R. G. M., Stedmon, C. A., Boehme, J. R., and Aiken,
934	G. R.: Measurement of Dissolved Organic Matter Fluorescence in Aquatic Environments:
935	An Interlaboratory Comparison, Environmental science & technology, 44, 9405-9412,
936	10.1021/es102362t, 2010.

- 937 Murphy, K. R., Hambly, A., Singh, S., Henderson, R. K., Baker, A., Stuetz, R., and Khan, S.
- J.: Organic matter fluorescence in municipal water recycling schemes: toward a unified
 PARAFAC model, Environmental science & technology, 45, 2909-2916,
- 940 10.1021/es103015e, 2011.
- Murphy, K. R., Stedmon, C. A., Graeber, D., and Bro, R.: Fluorescence spectroscopy and
 multi-way techniques. PARAFAC, Analytical Methods, 5, 6557, 10.1039/c3ay41160e,
 2013.
- 944 Nozière, B., González, N. J. D., Borg-Karlson, A.-K., Pei, Y., Redeby, J. P., Krejci, R.,
- 945 Dommen, J., Prevot, A. S. H., and Anthonsen, T.: Atmospheric chemistry in stereo: A
- new look at secondary organic aerosols from isoprene, Geophysical Research Letters, 38,
 n/a-n/a, 10.1029/2011gl047323, 2011.
- 948 Paglione, M., Saarikoski, S., Carbone, S., Hillamo, R., Facchini, M. C., Finessi, E.,
- 949 Giulianelli, L., Carbone, C., Fuzzi, S., Moretti, F., Tagliavini, E., Swietlicki, E., Eriksson
- 950 Stenström, K., Pr év α̂, A. S. H., Massoli, P., Canaragatna, M., Worsnop, D., and Decesari,
- 951 S.: Primary and secondary biomass burning aerosols determined by proton nuclear
- magnetic resonance (<sup>1</sup>H-NMR) spectroscopy during the 2008
- 953 EUCAARI campaign in the Po Valley (Italy), Atmospheric Chemistry and Physics, 14,
- 954 5089-5110, 10.5194/acp-14-5089-2014, 2014.

955	Park, SS., Sim, S. Y., Bae, MS., and Schauer, J. J.: Size distribution of water-soluble
956	components in particulate matter emitted from biomass burning, Atmospheric
957	Environment, 73, 62-72, 10.1016/j.atmosenv.2013.03.025, 2013.
958	Park, S. S., and Yu, J.: Chemical and light absorption properties of humic-like substances
959	from biomass burning emissions under controlled combustion experiments, Atmospheric
960	Environment, 136, 114-122, 10.1016/j.atmosenv.2016.04.022, 2016.
961	Pietrogrande, M. C., Bertoli, I., Clauser, G., Dalpiaz, C., Dell'Anna, R., Lazzeri, P., Lenzi, W.,
962	and Russo, M.: Chemical composition and oxidative potential of atmospheric particles
963	heavily impacted by residential wood burning in the alpine region of northern Italy,
964	Atmospheric Environment, 253, 118360, 10.1016/j.atmosenv.2021.118360, 2021.
965	Qin, J., Zhang, L., Zhou, X., Duan, J., Mu, S., Xiao, K., Hu, J., and Tan, J.: Fluorescence
966	fingerprinting properties for exploring water-soluble organic compounds in PM 2.5 in an
967	industrial city of northwest China, Atmospheric Environment, 184, 203-211,
968	10.1016/j.atmosenv.2018.04.049, 2018.
969	Sannigrahi, P., Sullivan, A. P., Weber, R. J., and Ingall, E. D.: Characterization of
970	water-soluble organic carbon in urban atmospheric aerosols using solid-state C-13 NMR
971	spectroscopy, Environmental science & technology, 40, 666-672, 10.1021/es051150i,
972	2006.
973	Santos, P. S., Otero, M., Duarte, R. M., and Duarte, A. C.: Spectroscopic characterization of
974	dissolved organic matter isolated from rainwater, Chemosphere, 74, 1053-1061,
975	10.1016/j.chemosphere.2008.10.061, 2009.

976 Santos, P. S., Santos, E. B., and Duarte, A. C.: First spectroscopic study on the structural 45

q	7	7

978

features of dissolved organic matter isolated from rainwater in different seasons, The Science of the total environment, 426, 172-179, 10.1016/j.scitotenv.2012.03.023, 2012.

Seo, I., Lee, K., Bae, M. S., Park, M., Maskey, S., Seo, A., Borlaza, L. J. S., Cosep, E. M. R., 979

- and Park, K.: Comparison of physical and chemical characteristics and oxidative 980 potential of fine particles emitted from rice straw and pine stem burning, Environmental 981 pollution, 267, 115599, 10.1016/j.envpol.2020.115599, 2020. 982
- Shen, G., Chen, Y., Wei, S., Fu, X., Zhu, Y., and Tao, S.: Mass absorption efficiency of 983 elemental carbon for source samples from residential biomass and coal combustions, 984

Atmospheric Environment, 79, 79-84, 10.1016/j.atmosenv.2013.05.082, 2013. 985

Singh, G. K., Choudhary, V., Rajeev, P., Paul, D., and Gupta, T.: Understanding the origin of 986 carbonaceous aerosols during periods of extensive biomass burning in northern India, 987 Environmental pollution, 270, 116082, 10.1016/j.envpol.2020.116082, 2021. 988

Sun, J., Zhi, G., Hitzenberger, R., Chen, Y., Tian, C., Zhang, Y., Feng, Y., Cheng, M., Zhang, 989

- Y., Cai, J., Chen, F., Qiu, Y., Jiang, Z., Li, J., Zhang, G., and Mo, Y.: Emission factors 990
- and light absorption properties of brown carbon from household coal combustion in 991 China, Atmospheric Chemistry and Physics, 17, 4769-4780, 10.5194/acp-17-4769-2017, 992

2017. 993

van der Werf, G. R., Randerson, J. T., Giglio, L., Collatz, G. J., Mu, M., Kasibhatla, P. S., 994

the contribution of deforestation, savanna, forest, agricultural, and peat fires (1997-2009),

Morton, D. C., DeFries, R. S., Jin, Y., and van Leeuwen, T. T.: Global fire emissions and

- Atmospheric Chemistry and Physics, 10, 11707-11735, 10.5194/acp-10-11707-2010, 997
- 2010. 998

995

Verma, V., Rico-Martinez, R., Kotra, N., King, L., Liu, J., Snell, T. W., and Weber, R. J.: 999 Contribution of water-soluble insoluble 1000 and components and their hydrophobic/hydrophilic subfractions to the reactive oxygen species-generating potential 1001 of fine ambient aerosols, Environmental science & technology, 46, 11384-11392, 1002 1003 10.1021/es302484r, 2012.

- Verma, V., Fang, T., Guo, H., King, L., Bates, J. T., Peltier, R. E., Edgerton, E., Russell, A. G.,
 and Weber, R. J.: Reactive oxygen species associated with water-soluble
 PM<sub>2.5</sub> in the southeastern United States: spatiotemporal trends
 and source apportionment, Atmospheric Chemistry and Physics, 14, 12915-12930,
 1008 10.5194/acp-14-12915-2014, 2014.
- Verma, V., Wang, Y., El-Afifi, R., Fang, T., Rowland, J., Russell, A. G., and Weber, R. J.:
 Fractionating ambient humic-like substances (HULIS) for their reactive oxygen species
 activity Assessing the importance of quinones and atmospheric aging, Atmospheric
 Environment, 120, 351-359, 10.1016/j.atmosenv.2015.09.010, 2015.
- Win, M. S., Tian, Z., Zhao, H., Xiao, K., Peng, J., Shang, Y., Wu, M., Xiu, G., Lu, S.,
 Yonemochi, S., and Wang, Q.: Atmospheric HULIS and its ability to mediate the reactive
 oxygen species (ROS): A review, Journal of environmental sciences, 71, 13-31,
- 1016 10.1016/j.jes.2017.12.004, 2018.
- 1017 Wong, J. P. S., Tsagkaraki, M., Tsiodra, I., Mihalopoulos, N., Violaki, K., Kanakidou, M.,
- 1018 Sciare, J., Nenes, A., and Weber, R. J.: Effects of Atmospheric Processing on the
- 1019 Oxidative Potential of Biomass Burning Organic Aerosols, Environmental science &
- technology, 53, 6747-6756, 10.1021/acs.est.9b01034, 2019.

- Wu, D., Wang, Z., Chen, J., Kong, S., Fu, X., Deng, H., Shao, G., and Wu, G.: Polycyclic
 aromatic hydrocarbons (PAHs) in atmospheric PM2.5 and PM10 at a coal-based
 industrial city: Implication for PAH control at industrial agglomeration regions, China,
 Atmospheric Research, 149, 217-229, 10.1016/j.atmosres.2014.06.012, 2014.
- 1025 Wu, G., Wan, X., Ram, K., Li, P., Liu, B., Yin, Y., Fu, P., Loewen, M., Gao, S., Kang, S.,
- Kawamura, K., Wang, Y., and Cong, Z.: Light absorption, fluorescence properties and
 sources of brown carbon aerosols in the Southeast Tibetan Plateau, Environmental
 pollution, 257, 113616, 10.1016/j.envpol.2019.113616, 2020.
- Wu, X., Liu, W., Gao, H., Alfaro, D., Sun, S., Lei, R., Jia, T., and Zheng, M.: Coordinated
 effects of air pollution control devices on PAH emissions in coal-fired power plants and
 industrial boilers, The Science of the total environment, 756, 144063,
 1032 10.1016/j.scitotenv.2020.144063, 2021.
- 1033 Yan, C., Zheng, M., Sullivan, A. P., Bosch, C., Desyaterik, Y., Andersson, A., Li, X., Guo, X.,
- 1034 Zhou, T., Gustafsson, Ö., and Collett, J. L.: Chemical characteristics and light-absorbing
- 1035 property of water-soluble organic carbon in Beijing: Biomass burning contributions,
- 1036 Atmospheric Environment, 121, 4-12, 10.1016/j.atmosenv.2015.05.005, 2015.
- 1037 Yu, S., Liu, W., Xu, Y., Yi, K., Zhou, M., Tao, S., and Liu, W.: Characteristics and oxidative
- 1038 potential of atmospheric PM2.5 in Beijing: Source apportionment and seasonal variation,
- 1039 The Science of the total environment, 650, 277-287, 10.1016/j.scitotenv.2018.09.021,
 1040 2019.
- 1041 Zhang, X., Lin, Y. H., Surratt, J. D., and Weber, R. J.: Sources, composition and absorption
- 1042 Angstrom exponent of light-absorbing organic components in aerosol extracts from the

- 1043 Los Angeles Basin, Environmental science & technology, 47, 3685-3693,
 1044 10.1021/es305047b, 2013.
- Zhu, J., Chen, Y., Shang, J., and Zhu, T.: Effects of air/fuel ratio and ozone aging on
 physicochemical properties and oxidative potential of soot particles, Chemosphere, 220,
- 1047 883-891, 10.1016/j.chemosphere.2018.12.107, 2019.
- 1048 Zou, C., Li, M., Cao, T., Zhu, M., Fan, X., Peng, S., Song, J., Jiang, B., Jia, W., Yu, C., Song,
- 1049 H., Yu, Z., Li, J., Zhang, G., and Peng, P. a.: Comparison of solid phase extraction
- 1050 methods for the measurement of humic-like substances (HULIS) in atmospheric
- 1051 particles, Atmospheric Environment, 225, 117370, 10.1016/j.atmosenv.2020.117370,
- 1052 2020.

			Bioma	ass burning				C	oal combusti	on	
Contents (%)	WS	RS	CS	PW	CR	WP	B-1	B-2	B-3	B-4	AN
OC	44±5.6	41±12	24±6.4	19±3.8	26±8.7	23±13	61±5.4	64±11	68±7.6	69±6.9	9.5±5.0
EC	2.5±0.9	1.3±0.6	4.4±2.8	10±3.4	5.0±3.3	13±7.6	0.2±0.1	1.1±0.8	0.3±0.1	0.8±0.6	0.1±0.0
TC^{a}	46±5.5	42±12	28±8.2	29±4.0	32±9.6	36±19	61±5.4	65±11	69±6.7	69±6.8	9.5±5.0
WSOC/PM ^b	11±2.7	12±1.6	9.7±0.2	3.9±1.1	7.6±0.3	2.9±0.7	15±0.4	22±4.1	9.2±1.5	4.7±0.4	2.3±1.1
HULIS-C/PM ^b	6.7±1.3	7.8 ± 0.2	4.0±0.5	1.7±0.3	3.1±0.6	1.0±0.4	6.0±0.6	10±0.8	4.2±0.4	2.0±0.2	0.5±0.1
MSOC/PM ^b	40±0.9	47±0.8	20±1.4	12±1.2	15±0.9	6.4±0.7	57±5.4	73±2.9	65±6.8	71±0.7	9.4±5.7
WSOC/TC ^c	22±6.0	23±3.0	25±3.0	14±3.1	32±3.0	21±9.4	25±2.9	29±4.3	14±3.2	6.4±0.5	22±8.5
HULIS-C/TC ^c	14±2.8	14±0.4	11±2.7	5.9±0.8	13±1.6	9.8±1.1	10±0.3	13±1.7	6.3±0.9	2.8±0.3	6.9±2.9
MSOC/TC ^c	82±2.2	88±1.5	57±11	53±7.5	78±16	52±27	99±0.2	95±1.9	98±0.1	96±0.1	95±1.8
HULIS-C/WSOC ^c	64±6.9	65±8.0	42±6.2	43±5.4	41±6.6	32±6.3	41±4.9	46±9.4	46±9.6	43±6.0	33±7.8
WSOC/OC ^c	23±5.9	23±3.1	33±0.9	24±4.0	36±2.6	35±3.2	25±2.9	30±4.5	14±3.3	6.4±0.5	26±3.9
HULIS-C/OC ^c	15±2.9	15±0.4	14±1.7	10±0.7	15±1.9	11±3.2	10±0.3	13±1.6	6.4±0.9	2.8±0.3	6.9±3.0
MSOC/OC ^c	88±1.9	91±1.2	70±4.5	76±2.5	72±6.7	77±4.5	99±0.1	96±0.5	98±0.1	98±0.5	96±1.6

Table 1. The contributions of BrC fraction (WSOC, HULIS, and MSOC) in smoke samples (%).

^a Total Carbon: sum of OC and EC

 b The ratios of the mass of carbon (µgC) to the mass of PM (µg) for each sample.

1057 ^c The ratios of the mass of carbon (μ gC) to the mass of carbon (μ gC) for each sample.

			WSC	C			HU	LIS			MS	OC	
	Samples	R-H	H-C-C=	H-C-O	Ar-H	R-H	H-C-C=	H-C-O	Ar-H	R-H	H-C-C=	H-C-O	Ar-H
		0.6-2.0 ^a	2.0-3.2	3.4-4.4	6.5-8.5	0.6-2.0	2.0-3.2	3.4-4.4	6.5-8.5	0.6-2.0	2.0-3.2	3.4-4.4	6.5-8.5
Biomass	WS	16 ^b	27	42	14	19	32	21	27	44	26	16	14
burning	RS	24	27	34	14	26	31	14	29	46	30	13	11
	CS	15	22	46	17	18	28	31	24	47	29	15	9
	PW	14	22	48	17	15	25	42	18	40	30	19	11
	CF	11	17	54	18	14	26	36	23	41	28	18	13
	WP	12	22	48	19	14	21	31	34	44	29	17	10
Coal	B-1	18	41	9.0	32	17	40	5.0	37	40	28	2.0	30
combustion	B-2	17	35	22	25	26	39	5.0	30	33	30	3.0	33
	B-3	17	39	14	30	22	34	8.0	35	34	30	2.0	33
	B-4	13	27	34	25	20	36	13	30	32	27	3.0	39
	AN	15	33	20	32	18	37	12	33	38	28	2.0	32

Table 2. The proton species in the BrC fractions (WSOC, HULIS, and MSOC) of smoke samples.

1062 ^a chemical shift: ppm. ^b percentage of each type of protons (%).

	DTT	OC
_	R	р
MAE ₃₆₅	0.697**	0.000
Fluorescence component 1 (%) ^b	-0.078	0.668
Fluorescence component 2 (%) ^b	-0.330	0.061
Fluorescence component 3 (%) ^b	0.151	0.402
Fluorescence component 4 (%) ^b	0.560**	0.001
R-H (%)	0.697**	0.000
H-C=C (%)	-0.247	0.166
H-C-O (%)	-0.223	0.213
Ar-H (%)	-0.345*	0.049

Table 3. Pearson correlation coefficient analysis between oxidation potential and chemical characteristics of BrC

1067 a: DTT_{OC} were calculated using the DTT consumption rate divided by the mass of organic carbon.

b: fluorescence component 1-4 poresent fluorophores 1-4 (C_W 1-4 and C_M 1-4) identified by PARAFAC method

1069 ** There was significant correlation in 99% confidence interval (bilateral) (p value no more than 0.01).

1070 * There was significant correlation in 95% confidence interval (bilateral) (p value no more than 0.05).

1071

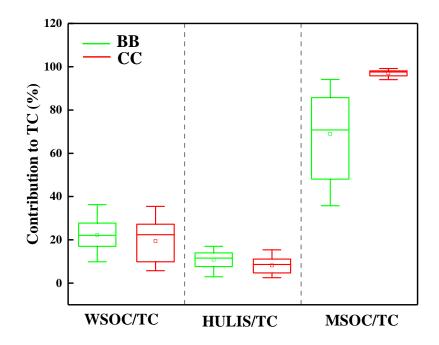


Figure 1. The abundances of BrC fraction in the smoke samples from biomass burning (BB) and coal combustion (CC)

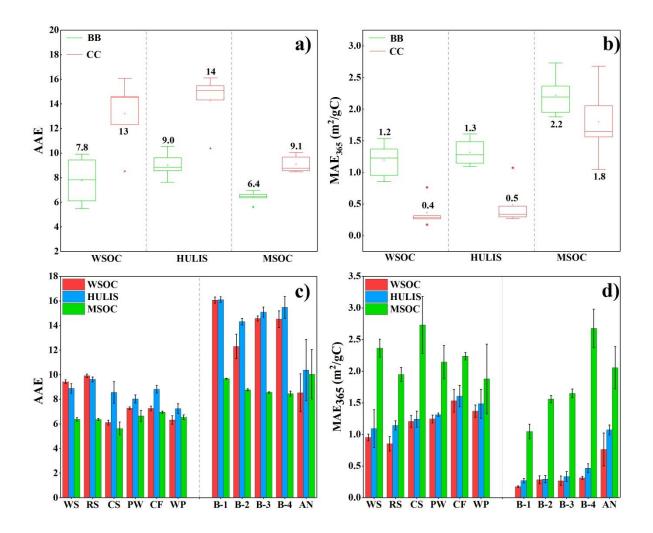


Figure 2. The AAE and MAE_{365} values of WSOC, HULIS, and MSOC in smoke samples from biomass burning (BB) and coal combustion (CC)

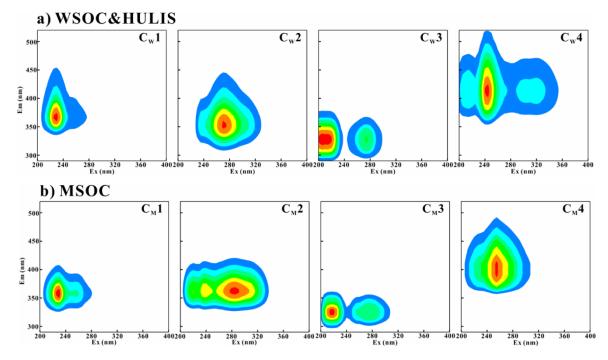


Figure 3. Four fluorescence components identified by PARAFAC analysis of a) WSOC, HULIS ($C_W1:C_W4$); b) MSOC ($C_M1:C_M4$) extracted from BB and CC smoke $PM_{2.5}$ (normalized in Raman unit, R.U.)

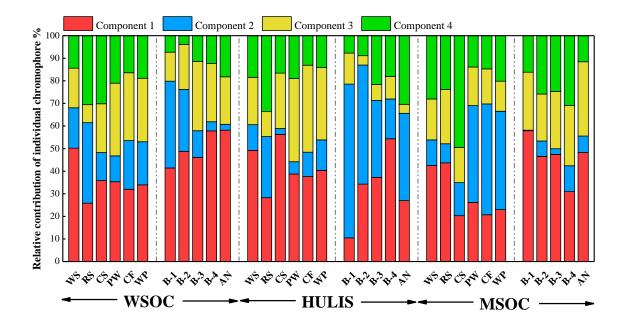


Figure 4. Relative contribution calculated by F_{max} of individual chromophores analyzed by PARAFAC. Component 1-4 represent C_w1-4 for water-soluble BrC (WSOC and HULIS) and and C_M1-4 for methanol-soluble BrC (MSOC), respectively.

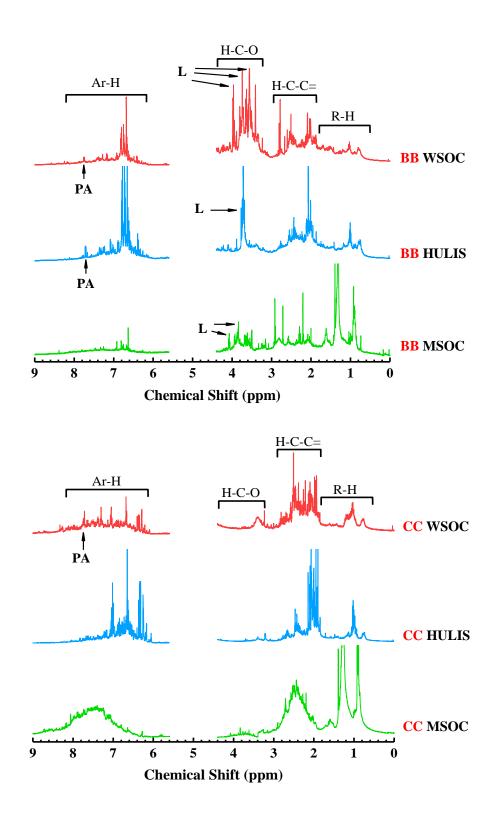


Figure 5. ¹H NMR spectra of WSOC, HULIS, and MSOC in typical biomass burning and coal combustion smoke samples (BB: wheat straw; CC: B-1 coal). The segment from 4.40 to 5.60 ppm was removed for NMR spectra due to MeOH and H_2O residues. The peaks were assigned to specific compounds as follows: Levoglucosan (L), Phthlic acid (PA).

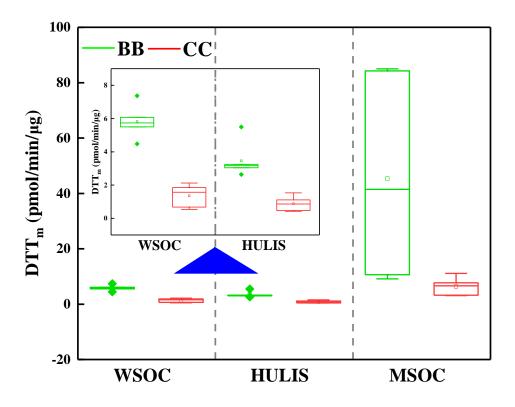


Figure 6. Results of DTT assay conducted on the WSOC, HULIS and MSOC of smoke $PM_{2.5}$, the values were normalized by the mass of smoke $PM_{2.5}$. Above the blue triangle symbol is the result coordinates of WSOC and HULIS to be enlarged.

